Phase Error Correction for Multiple Planes using Sharpness Metrics

Abbie E. Tippie and James R. Fienup*
Institute of Optics, University of Rochester, Rochester, NY 14627

ABSTRACT

Phase errors introduced in the object beam of a digital hologram degrade the image quality of the object. We present computer simulations showing the effect of multiple planes of phase errors in the propagation path. By using a nonlinear optimization technique to maximize sharpness metrics, we show results that account for aberrations in multiple planes and correct anisoplanatic blur. This paper demonstrates this technique for two and three phase screens.

Keywords: anisoplanatic imaging, atmospheric turbulence, phase screen, sharpness metric, volume turbulence, digital holography

1. INTRODUCTION

Imaging through volume turbulence can have adverse effects on image quality. Each ray of light that traverses through the propagation medium will experience different optical path lengths due to changes in refraction index as a result of the turbulent atmosphere. Spatially-variant (anisoplanatic) imaging will occur due to the ray bundles from different object points passing through different volumes of turbulence. The effect of anisoplanatism is present in a wide range of imaging scenarios including horizontal path imaging through the atmosphere, adaptive optics using a laser guide star [1] and even the human eye [2].

Recent work has examined anisoplanatic imaging using digital holography [3, 4]. In these papers, the effect of anisoplanatism occurred when the optical fields propagated through an aberrated phase media in one discrete plane. Thurman and Fienup were able to correct for the anisoplanatism with the use of sharpness metrics. Results were shown for both simulation and experiment. In this paper, we extend the previous research to account for phase errors in multiple planes. We discuss a simulation which models this anisoplanatic imaging scenario. We then describe a nonlinear optimization technique using a sharpness metric to estimate the volume turbulence and correct the spatially variant blur in the image.

2. OPTICAL MODEL

The forward model for our simulation is a digital holography experiment [3, 4] illustrated in Figure 1. The object is illuminated with a coherent laser. The coherent light reflected from the object creates a random phase, speckled field (this allows us to not be too concerned with the propagation of the illumination beam through the turbulence) which propagates to the first plane of turbulence. In each plane of turbulence, the speckled field is multiplied by the transmittance of a phase screen introducing phase errors in that plane. After propagating the object field to the plane of the detector, we interfere the field with a reference plane wave in order to perform digital holography. We inverse transform the detected intensity and window out the object term, G_{hol}. Using digital holography for imaging allow us to have access to both the magnitude and the phase of the coherent optical field. Heterodyne detection would be an alternative to digital holography. We can back propagate the field G_{hol}, multiplying by the phase screens to reconstruct the field in the object plane. Reconstructions using the phase estimates are found by the sharpness metric technique. Since this

* email: fienup@optics.rochester.edu, phone: (585) 275-8009

Unconventional Imaging IV, edited by Jean J. Dolne, Thomas J. Karr, Victor L. Gamiz,
Proc. of SPIE Vol. 7094, 709404, (2008) · 0277-786X/08/$18 · doi: 10.1117/12.795193

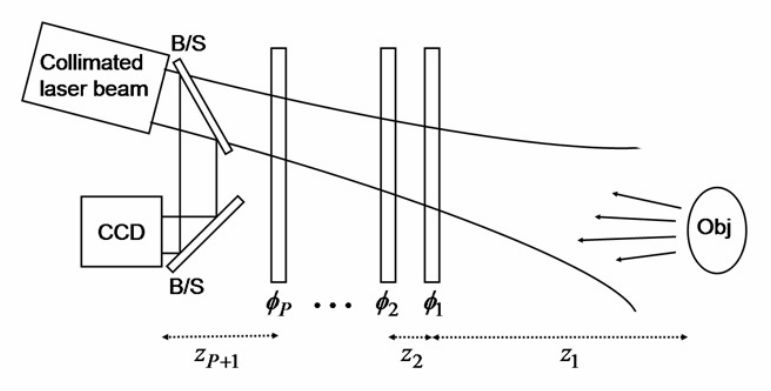

Figure 1. Digital holography experimental setup for imaging through multiple layers of turbulence.

work is done in simulation, we will be able to check our reconstruction results with truth by forming an ideal image of the object using the exact phase maps.

In order to model the volume turbulence in simulation, we choose to discretize the turbulence. Appropriate use of discrete phase screens to model volume turbulence has been shown to be statistically equivalent to true volume turbulence [5,6]. For the p^{th} phase screen, the phase estimate is

$$\hat{\phi}_p(x,y) = \sum_j c_{p,j}\psi_j(x,y) \tag{1}$$

where j is the index for the basis function $\psi_j(x,y)$ and $c_{p,j}$ are the expansion coefficients.

3. NONLINEAR OPTIMIZATION

The technique to estimate the phase, as we have alluded to previously, is a nonlinear optimization technique using a sharpness metric. The use of sharpness metrics for improving imagery was pioneered by Muller and Buffington [7]. More recently, sharpness metrics have been used for coherent imaging [3,4,8-11]. Variations and use of the designer metrics have shown that an appropriate sharpness metric is dependent on the properties of the object and the scene conditions [3,11]. For this work, we use an I^β sharpness metric, where $\beta = 1.01$ and I is the intensity of the speckle-averaged image which can be described as

$$I(\xi,\eta) = \frac{1}{K}\sum_{k=1}^{K}\left|f_k(\xi,\eta)\right|^2 \tag{2}$$

where $f_k(\xi,\eta)$ is the object field for the k^{th} speckle realization. The sharpness metric, S, in this case is an integral over I^β. For conjugate-gradient nonlinear optimization, we derive $\partial S / \partial \hat{\varphi}_p$, the partial derivative of the sharpness metric with respect to the phase of the p^{th} phase screen in order to make the algorithm computationally efficient.

We introduce some useful propagators in order to simplify notation. We denote the paraxial angular spectrum propagation of an arbitrary field $g(x,y)$ at a distance z as

$$\mathcal{A}\left[z; g(x,y)\right] = FT^{-1}\left\{FT\left[g(x,y)\right]\exp\left[-i\pi\lambda z\left(f_x^2 + f_y^2\right)\right]\right\} \tag{3}$$

where *FT* denotes a discrete Fourier transform. In order to propagate an object field $f_k(\xi,\eta)$ to a plane immediately before the p^{th} phase screen, we define the propagator

$$\mathcal{P}_{1\to p_-}\left[f_k(\xi,\eta)\right]=\mathcal{A}\left\{z_p;\exp\left(i\phi_{p-1}\right)\cdots\mathcal{A}\left[z_3;\exp\left(i\phi_2\right)\mathcal{A}\left\{z_2;\exp\left(i\phi_1\right)\mathcal{F}_r\left[z_1;f_k(\xi,\eta)\right]\right\}\right]\cdots\right\} \tag{4}$$

where $\mathcal{F}_r\left[z_1;f_k(\xi,\eta)\right]$ is a Fresnel transform of the object field propagated a distance z_1 to the first phase screen. Similarly, we define an inverse propagator as

$$\begin{aligned}\mathcal{P}^{\dagger}_{P+1\to p_-}\left[G_k(u,v)\right]=\exp\left(-i\phi_p\right)\mathcal{A}\Big[-z_{p+1};\exp\left(-i\phi_{p+1}\right)\cdots\mathcal{A}\left\{-z_{P-1};\exp\left(-i\phi_{P-1}\right)\right.\\ \left.\times\mathcal{A}\left[-z_P;\exp\left(-i\phi_P\right)\mathcal{A}\left\{-z_{P+1};G_k(u,v)\right\}\right]\right\}\cdots\Big]\end{aligned} \tag{5}$$

where we now propagate backward from the detector plane through *P-p* phase screens, where *P* is the total number of phase screens and *p* is the phase screen which we are optimizing. The partial derivative of the sharpness metric with respect to the value of the phase at point (*x,y*) in the p^{th} phase screen can be shown to be

$$\frac{\partial S}{\partial\phi_p(x,y)}=-\frac{2}{K}\sum_{k=1}^{K}\operatorname{Im}\left(\mathcal{P}_{1\to p_-}\left[\beta I^{\beta-1}(\xi,\eta)f_k(\xi,\eta)\right]\left\{\mathcal{P}^{\dagger}_{P+1\to p}\left[G_k(u,v)\right]\right\}^{*}\right) \tag{6}$$

where *K* is the number of speckle realizations. This allows efficient calculation of the entire gradient of the sharpness metric. The gradients with respect to the polynomial coefficient $c_{p,j}$ can be gotten by taking the inner product of Eq. (6) with the basis function.

4. SIMULATION EXPERIMENTS

In this section we discuss the specific parameters used in the simulation results presented Section 5 of this paper. The object used in this work was a 256x256 incoherent intensity image (an aerial photograph of an urban area). We multiplied its square root by circular, complex Gaussian random numbers in order to form a complex object speckle realization. The complex object was zero-padded to an array size of 1024x1024, and this field was Fourier transformed and cropped to the original object array size. This Fourier transform represents a Fraunhofer propagation from the object to the first phase screen, as would be true, for example, for imaging earth-orbiting satellites from the ground. The field was then multiplied by a 256x256 pixel phase screen. Angular spectrum propagation was used for each propagation between phase screens, as described above. For these simulations, the inter-screen distance between the phase screens was 100 m, i.e. $z_2 = z_3 = 100$ m for the two-screen case and $z_2 = z_3 = z_4 = 100$ m for the three-screen case.

In the plane of the detector, an off-axis plane wave was added to the aberrated field and the intensity of the resulting hologram was computed. The angle of the off-axis plane wave was chosen to avoid overlap of the desired term with the autocorrelation term. For these initial experiments no noise was added; previous experiments [3, 4] showed that sharpness maximization was robust in the presence of noise. Using the holography data, the object term was windowed out using a cosine guard band around the edges to reduce ringing artifacts. We used $K = 24$ independent speckle realizations for the intensity in Eq. (2).

The phase screens used in this simulation are 15th order polynomial versions of a Kolmogorov screen, based on work in Ref [12]. The phase maps reconstructed using the nonlinear optimization technique are also 15th order polynomials. The index structure constant C_n^2 is related to Fried's parameter r_0 by [13]

$$r_0 = 1.678\left(k^2 \int_0^L dz C_n^2(z) \right)^{-3/5} \tag{7}$$

where $k = 2\pi / \lambda$. An overall Fried's parameter r_0 and the Fried's parameters of individual turbulence layers r_{0i} are related by [13]

$$r_0^{-5/3} = \sum_{i=1}^{N} r_{0i}^{-5/3} \ . \tag{8}$$

We chose to maintain the same Fried's parameter for each individual turbulence layer.

Our approach to recover the phase of each plane of turbulence was to maximize the sharpness metric by optimizing over the lowest order polynomial coefficients first and increasing the order later. For the initial guess of each phase screen, we set each polynomial coefficient equal to zero. We first performed eight conjugate-gradient (CG) iterations using only the 3rd order terms. After finding estimates for those coefficient values, we performed eight additional CG iterations including the 4th order terms. We continued this process of slowly adding higher order polynomial terms and optimizing over their coefficients, up to the 15th order terms. For this simulation, both the true phase maps and estimated phase maps were of the same polynomial order, and we optimized over phase screens in the same location as those used to simulate the measured data. Extension of this optimization technique to a point-by-point phase map reconstruction of a Kolmogorov screen has been demonstrated [3].

5. RESULTS

The results of this technique are presented in Figures 2 and 3. Figure 2 shows the algorithm's ability to reconstruct the correct phase. For the object, propagation distances and specific phase screens used in this

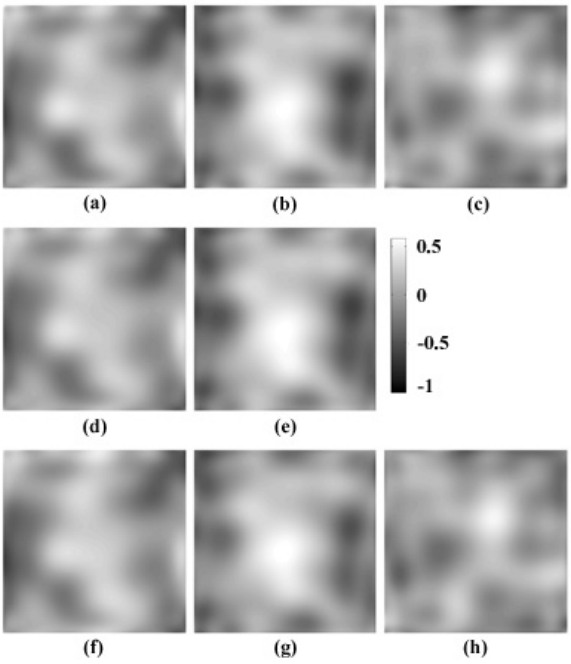

Figure. 2. Phases for the two- and three-screen simulations. Simulated true phase for (a) plane 1, (b) plane 2 and (c) plane 3 (only present in the three-screen simulation). 15th order polynomial phase estimates found through image sharpening technique for (d) – (e) the two-screen simulation and (f) – (h) the three-screen simulation. The scale is given in units of waves.

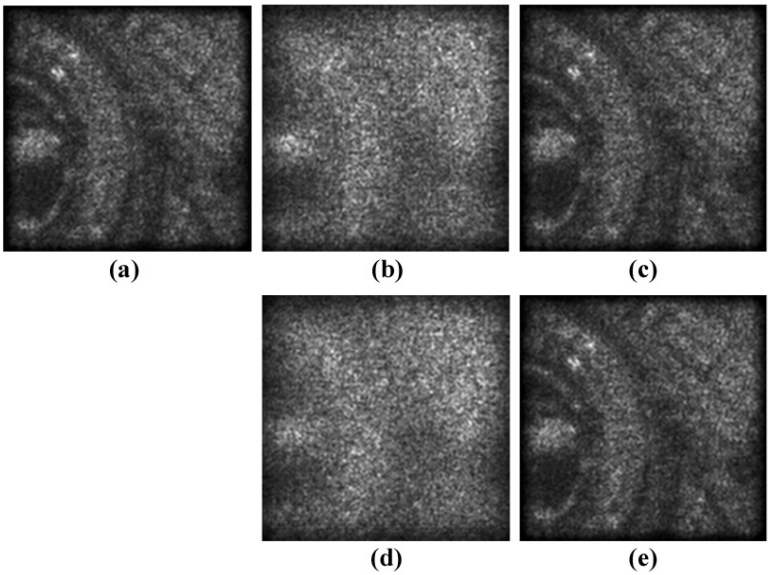

Figure. 3. Results for the two- and three-screen simulations. (a) The ideal image. Two-screen simulation when (b) there is no aberration correction and (d) the phase estimates have been used in the reconstruction. Three-screen simulation for (d) the aberrated image and (e) the image reconstructed with phase estimates.

simulation, the reconstructed phase screens for both the two and three screen cases show good agreement with the actual phase screens. The algorithm's ability to reconstruct phase maps that match the true phase screens strongly depends on the total propagation distance and thus the propagation distance from one screen to the next. We found that when the distance between phase screens was relatively small (compared to the z_p = 100 m shown in Fig. 2) the reconstructed phase maps did not agree with the true phase. However, in these instances, the sum of two phase maps agreed with the sum of the two true phase maps. This is to be expected since phase screens very close to one another act like a single phase screen with phase equal to the sum of the two phases. Due to this fact, an error metric was chosen to compare the true and reconstructed object, as opposed to the individual phase screens. The absolute error of the images was computed by [14,15]

$$E^2 = \min_{\xi_0,\eta_0}\left\{\frac{\sum_{\xi,\eta}\left|\hat{I}(\xi-\xi_0,\eta-\eta_0)-I(\xi,\eta)\right|^2}{\sum_{\xi,\eta}\left|I(\xi,\eta)\right|^2}\right\} \tag{9}$$

where $\hat{I}(\xi,\eta)$ is intensity of the reconstructed image and $I(\xi,\eta)$ is the intensity of the ideal image. Figure 3(a) shows the ideal image and Figs. 3(c) and 3(e) show the reconstructed images for the two- and three-screen cases, respectively. We also show in Fig. 3(b) and 3(d) the resulting blurred image if turbulence is not accounted for and corrected. In the presence of turbulence, the image is severely blurred, and the absolute error for these uncorrected images was 0.3264 and 0.3311 for the two-screen and three-screen simulations, respectively. Both reconstructed images are far superior to the uncorrected image and both match the true object relatively well. Quantitatively, the absolute error for the reconstructed images was 0.0643 and 0.0813 for the two- and three-screen case, respectively. This reduction in the absolute error metric helps demonstrate the ability of this nonlinear optimization approach to correct for phase errors in multiple planes of turbulence and correct anisoplanatic blur.

6. CONCLUSION

We have successfully demonstrated the ability to correct for anisoplanatic blur with image sharpening of digital holography data. This space-variant image correction was achieved using a nonlinear optimization sharpness maximization technique. Through this optimization process, we were able to form estimates of the phase aberrations in multiple planes and use those phases to appropriately reconstruct an object estimate, thereby correcting anisoplanatic blur.

In the future we will perform simulations of higher fidelity including the effects of noise and measures to avoid aliasing in the digital propagations. Additionally, we would like to further investigate relevant parameters and improve the nonlinear optimization to allow for optimization with respect to unknown location of phase screens or increase the computational efficiency of the technique as the number of phase screens increases. We hope to verify results in the laboratory setting since we have seen promising results in simulation for this technique.

REFERENCES

[1] Welsh, B. M. and Gardner, C. S., "Effects of turbulence-induced anisoplanatism on the imaging performance of adaptive-astronomical telescopes using laser guide stars," J. Opt. Soc. Am. A **8**, 69-80 (1991).

[2] Dubinin A., Belyakov A., Cherezova T., Kudryashov A., "Anisoplanatism in human retina imaging," Proc. SPIE **5894**, 88-94, (2005).

[3] Thurman, S. T. and Fienup, J. R., "Phase-error correction in digital holography," J. Opt. Soc. Am. A **25**, 983-994 (2008).

[4] Thurman, S. T. and Fienup, J. R., "Correction of anisoplanatic phase errors in digital holography," J. Opt. Soc. Am. A **25**, 995-999 (2008).

[5] Booker, H.G., Ferguson, J.A. and Vats, H.O., "Comparison between the extended-medium and the phase-screen scintillation theories," Jrnl. of Atmos. and Terr. Phys. **47**, 381-399 (1985).

[6] Andrews, L.C. and Phillips, R. L., Laser Beam Propagation through Random Media (SPIE Press, 2005).

[7] Muller, R. A. and Buffington, A., "Real-time correction of atmospherically degraded telescope images through image sharpening," J. Opt. Soc. Am. **64**, 1200-1210 (1974).

[8] Paxman, R. G. and Marron, J. C., "Aberration correction of speckled imagery with an image-sharpness criterion," Proc. SPIE **976**, 37-47 (1988).

[9] Berizzi, F. and Corsini, G., "Autofocusing of inverse synthetic aperture radar images using contrast optimization," IEEE Trans. Aerosp. Electron. Sys. **32**, 1185-1191 (1996).

[10] Fienup, J.R., "Synthetic-Aperture Radar Autofocus by Maximizing Sharpness," Opt. Lett. **25**, 221-223 (2000).

[11] Fienup, J.R. and Miller, J.J., "Aberration Correction by Maximizing Generalized Sharpness Metrics," J. Opt. Soc. Am. A, **20**, 609-620 (2003).

[12] Lane, R. G., Glindemann, A. and Dainty, J. C., "Simulation of a Kolmogorov phase screen," Waves in Random Media **2**, 209-224 (1992).

[13] Roggemann, M. C. and Welsh, B. M., Imaging through Turbulence, (CRC Press, 1996).

[14] Fienup, J. R., "Invariant error metrics for image reconstruction," Appl. Opt. **36**, 8352-8357 (1997).

[15] Guizar-Sicairos, M., Thurman, S.T. and Fienup, J.R., "Efficient Subpixel Image Registration Algorithms," Opt. Lett. **33**, 156-158 (2008).